the plant journal

SEB Society for Experimental Biology

The Plant Journal (2018) **94,** 1083–1097 doi: 10.1111/tpj.13921

A chromatin loop represses *WUSCHEL* expression in Arabidopsis

Lin Guo[1,2,†], Xiuwei Cao[1,2,†], Yuhao Liu[3,†], Jun Li[4], Yongpeng Li[1,2], Dongming Li[1,2], Ke Zhang[1,2], Caixia Gao[4], Aiwu Dong[3] and Xigang Liu[1,2,*]

[1]*State Key Laboratory of Plant Cell and Chromosome Engineering, Center for Agricultural Resources Research, Institute of Genetics and Developmental Biology, Chinese Academy of Sciences, Shijiazhuang, China,*
[2]*Hebei Collaboration Innovation Center for Cell Signaling, Shijiazhuang 050021, China,*
[3]*State Key Laboratory of Genetic Engineering, International Associated Laboratory of CNRS-Fudan-HUNAU on Plant Epigenome Research, Collaborative Innovation Center for Genetics and Development, Institute of Plant Biology, School of Life Sciences, Fudan University, Shanghai 200433, China, and*
[4]*State Key Laboratory of Plant Cell and Chromosome Engineering, Institute of Genetics and Developmental Biology, Chinese Academy of Sciences, Beijing 100101, China*

Received 30 November 2017; revised 20 March 2018; accepted 22 March 2018; published online 16 April 2018.
*For correspondence (e-mail xgliu@sjziam.ac.cn).
†These authors contributed equally to this work.

SUMMARY

***WUSCHEL* (*WUS*) is critical for plant meristem maintenance and determinacy in Arabidopsis, and the regulation of its spatiotemporal expression patterns is complex. We previously found that AGAMOUS (AG), a key MADS-domain transcription factor in floral organ identity and floral meristem determinacy, can directly suppress *WUS* expression through the recruitment of the Polycomb group (PcG) protein TERMINAL FLOWER 2 (TFL2, also known as LIKE HETEROCHROMATIN PROTEIN 1, LHP1) at the *WUS* locus; however, the mechanism by which *WUS* is repressed remains unclear. Here, using chromosome conformation capture (3C) and chromatin immunoprecipitation 3C, we found that two specific regions flanking the *WUS* gene body bound by AG and TFL2 form a chromatin loop that is directly promoted by AG during flower development in a manner independent of the physical distance and sequence content of the intervening region. Moreover, AG physically interacts with TFL2, and TFL2 binding to the chromatin loop is dependent on AG. Transgenic and CRISPR/Cas9-edited lines showed that the *WUS* chromatin loop represses gene expression by blocking the recruitment of RNA polymerase II at the locus. The findings uncover the *WUS* chromatin loop as another regulatory mechanism controlling *WUS* expression, and also shed light on the factors required for chromatin conformation change and their recruitment.**

Keywords: AGAMOUS, chromatin conformation capture, chromatin loop, TERMINAL FLOWER 2, WUSCHEL, Arabidopsis.

INTRODUCTION

Stem cells are critical for morphogenesis in multicellular organisms, and the mechanisms underlying stem cell maintenance and termination are key developmental concerns. In both plants and animals, stem cell niches produce conserved maintenance factors to repress stem cell differentiation (Scheres, 2007). In the model plant Arabidopsis, stem cells are located at the tips of meristems. Maintenance of their stemness property requires the homeobox gene *WUSCHEL* (*WUS*), the expression of which is restricted to a small group of cells underneath the stem cells known as the organizing center (OC) (Laux *et al.*, 1996; Mayer *et al.*, 1998). *WUS* plays a vital role in the establishment and maintenance of both the shoot apical meristem (SAM) and the floral meristem (FM), as well as in FM termination (Laux *et al.*, 1996; Mayer *et al.*, 1998; Gallois *et al.*, 2004; Sun *et al.*, 2009; Liu *et al.*, 2011). In the FM, stem cell activity is terminated along with the suppression of *WUS* expression once the carpel primordia are initiated at stage 6 of flower development, to ensure subsequent carpel development (Smyth *et al.*, 1990; Lenhard *et al.*, 2001). Transiently or persistently prolonged *WUS* expression results in FM determinacy, which is characterized by supernumerary whorls or additional tissue growing inside the primary gynoecium (Sablowski, 2007;

Prunet *et al.*, 2009). *AGAMOUS* (*AG*) encodes a MADS-domain transcription factor (TF) and is the central player in promoting FM determinacy by repressing *WUS* expression (Yanofsky *et al.*, 1990). In the *ag-1* null mutant, de-repressed *WUS* expression beyond stage 6 results in a flower-in-flower phenotype (Lenhard *et al.*, 2001). It was more recently shown that AG can suppress *WUS* expression through direct and indirect means (Cao *et al.*, 2015; Sun and Ito, 2015). Specifically, AG was found to inhibit *WUS* expression directly through the recruitment of the Polycomb group (PcG) protein TERMINAL FLOWER 2 (TFL2, also known as LIKE HETEROCHROMATIN PROTEIN 1, LHP1) at the *WUS* locus (Liu *et al.*, 2011), and indirectly by activating *KNUCKLES* (*KNU*) expression and consequently repressing *WUS* expression (Sun *et al.*, 2009, 2014). Although the indirect regulation of *WUS* by *AG* is well characterized, the mechanism by which *AG* directly represses *WUS* warrants further study.

Regulatory information about gene expression is encoded in the defined DNA sequences known as *cis*-regulatory elements (CREs), which have critical roles in controlling gene expression in specific cell types and developmental stages (Li *et al.*, 2015). A previous analysis of the *WUS* promoter using the b-glucuronidase (*GUS*) reporter aimed to identify the regions controlling the spatiotemporal transcription pattern of *WUS*. Distinct regulatory domains in the *WUS* promoter were found to be essential for the *WUS* expression pattern in the ovule, FM and inflorescence meristem, as well as for the enhancement of the expression level of *WUS* (Baurle and Laux, 2005). Besides the promoter region, a region downstream of the *WUS* 3′ untranslated region (UTR) is also important for *WUS* expression regulation (Liu *et al.*, 2011). Specifically, we found that AG directly represses *WUS* expression by binding to the transcription start site (TSS) of *WUS* and the region downstream of the *WUS* 3′-UTR (hereafter referred to as *WUS* 5′-TSS and *WUS* 3′-CRE, respectively). Further analysis of the *WUS* 3′-CRE region revealed that it contains two tandem CArG box motifs that may be bound by MADS domain-containing proteins (Huang *et al.*, 1993; Shiraishi *et al.*, 1993), but there is presently no definitive evidence of AG binding specifically to these CArG boxes in the *WUS* 3′-CRE. Mutations in the CArG boxes resulted in prolonged *WUS* expression in a *WUS:GUS:WUS3′mut* reporter line, however, indicating that the *WUS* 3′-CRE is important for the precise regulation of *WUS* expression in FM determinacy (Liu *et al.*, 2011). This finding was reinforced by subsequent findings from a functional analysis of TOPOISOMERASE 1α (TOP1α), a type-I DNA topoisomerase. In the *top1α* mutant, nucleosome density is increased at the *WUS* 3′-CRE, impairing AG binding to *WUS* and resulting in an enhanced FM determinacy defect (Liu *et al.*, 2014). Exactly how AG interacts with CREs to regulate *WUS* expression remains unclear, however.

To establish the proper levels and expression patterns of a given gene, the regulatory information contained in CREs is decoded by diverse TFs that bind to them. These TFs often assemble multi-protein complexes and contain multiple interacting domains to trigger the formation of specific inter- or intra-chromosome connections, resulting in a cell type-specific three dimensional (3D) arrangement of chromatin (Gomez-Diaz and Corces, 2014). In mammals, chromatin and genome reorganization processes, along with DNA methylation, histone modification and nucleosome assembly, occur in embryonic stem cells (ESCs) in early differentiation (Mattout and Meshorer, 2010). In plants, MADS-box TFs, as one example, can form protein complexes to mediate chromatin interaction (Smaczniak *et al.*, 2012), and it is well established that the specific organization and folding of chromatin can dictate the proper expression of genes (Kadauke and Blobel, 2009; Matharu and Ahituv, 2015). With respect to plant cells, a recent genome-wide analysis of chromatin packing revealed that self-loops around genes are a common phenomenon in Arabidopsis (Liu *et al.*, 2016). Chromatin loops that are mediated by TFs and function in specific gene expression regulation in plants have also been reported (Louwers *et al.*, 2009; Crevillen *et al.*, 2013; Liu *et al.*, 2013; Ariel *et al.*, 2014; Cao *et al.*, 2014; Kim and Sung, 2017). Chromatin loops may have repressive or activating functions, and epigenetic factors may be involved in their formation (Kadauke and Blobel, 2009). Here, we demonstrate that a chromatin loop at the *WUS* locus, promoted in part by AG, represses *WUS* expression during flower development in Arabidopsis.

RESULTS

A chromatin loop exists at the *WUS* locus

Our previous study demonstrated that the *WUS* 3′-CRE region, containing two tandem CArG boxes, is important for *WUS* expression regulation (Figure 1a; Liu *et al.*, 2011). To investigate how the CArG boxes regulate *WUS* expression, we obtained the T-DNA insertion line SALK_114398 from the Arabidopsis Biological Resource Center (ABRC, https://abrc.osu.edu), and verified the site of the T-DNA insertion in the *WUS* 3′-UTR by PCR amplification and sequencing (Figure S1a). Wild-type (WT) and SALK_114398 inflorescences containing stage-8 and younger flowers were collected, and *WUS* transcript levels were measured using real-time quantitative PCR (qPCR). The *WUS* transcript levels were similar in the T-DNA insertion line and in the WT (Figure S1b). *In situ* hybridization was performed to assess the *WUS* expression pattern. In both the WT and the T-DNA insertion line, *WUS* was expressed in the OC in stage-3 flowers and was shut off at stage 6 (Figure S1c). Thus, neither the transcript abundance nor the spatiotemporal expression pattern of *WUS* was affected by the

T-DNA insertion in the *WUS* 3′-UTR, indicating that *WUS* regulation by the *WUS* 3′-CRE region may be independent of the physical distance on chromatin.

We therefore investigated whether the DNA spatial conformation known as a chromatin loop exists at the *WUS* locus and contributes to the complexity of *WUS* regulation using quantitative chromosome conformation capture (3C)-PCR experiments (Dekker *et al.*, 2002; Hagege *et al.*, 2007). WT inflorescences containing unopened flowers were collected and crosslinked with formaldehyde, followed by nuclear extraction. For these experiments, a non-crosslinked sample served as the negative control. Next, we fragmented the *WUS* locus DNA with *Dpn*II digestion, as illustrated in Figure 1a, and primers flanking the *WUS* 5′-TSS and *WUS* 3′-CRE regions were used to investigate the chromatin interactions (Figure 1a). The amplification efficiency for each primer combination was first examined to ensure comparable PCR products were obtained from each primer set (Figure S2). A1 and A2 were used as anchor primers in PCR reactions, to be paired with other primers located on the *WUS* locus (Figure 1a). Specific binding was not observed in the non-crosslinked control

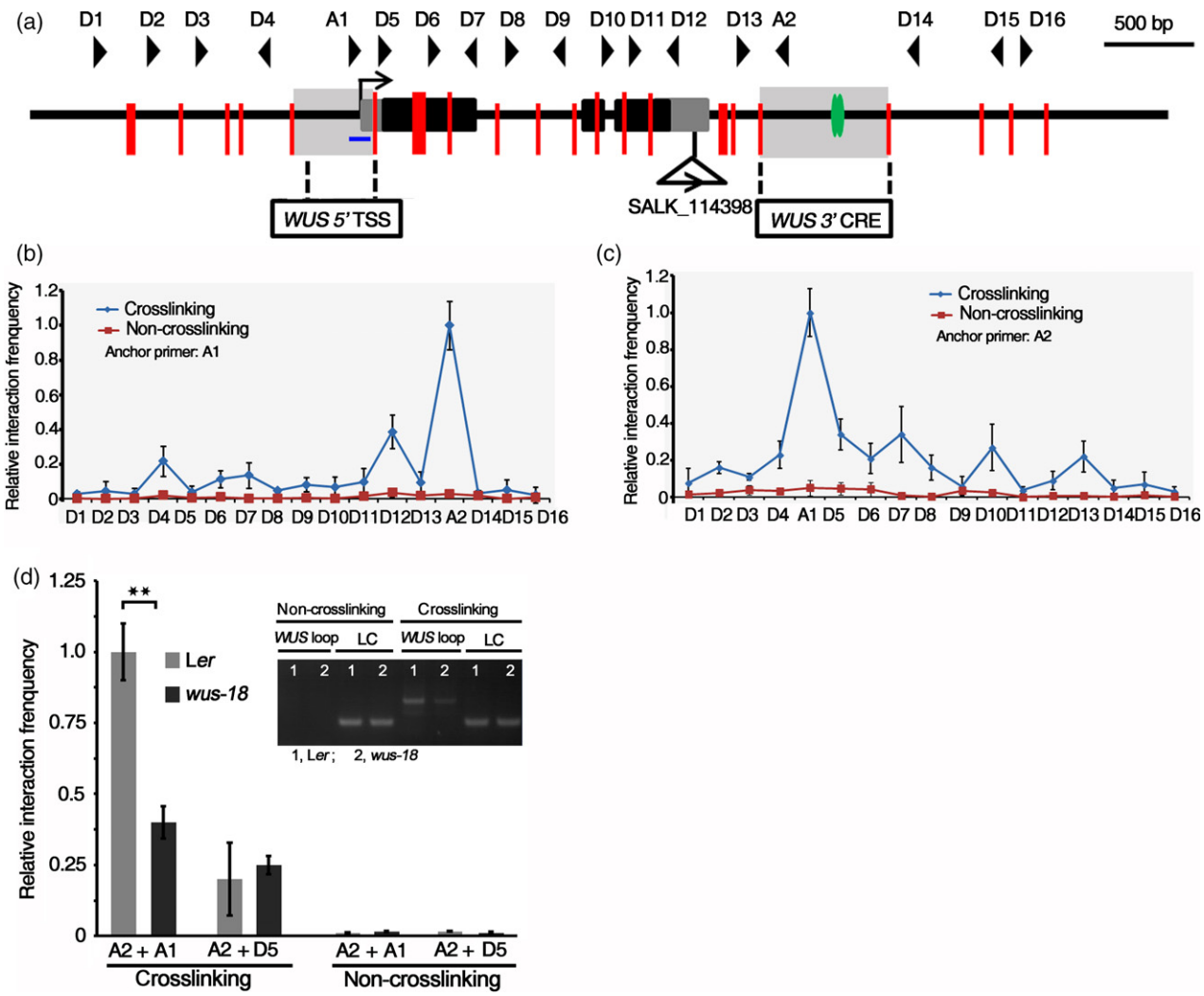

Figure 1. Chromatin loop at the *WUS* locus.
(a) Diagram of the *WUS* locus showing the *Dpn*II sites (red bars), primer locations (black triangles), CArG boxes (green ellipses) and the *WUS* 5′-TSS and *WUS* 3′-CRE regions, as well as the region that served as the loading control (LC) in this study (marked with a blue line). The anchor regions corresponding to A1 and A2 primers, respectively, are marked by the light-gray color. The anchor regions are examined in all 3C panels in this study, excepting Figure S3c–g.
(b, c) 3C-qPCR examining the chromatin loop at the *WUS* locus: A1 (b) or A2 (c) was used as the anchor primer in the PCR reaction to be paired with other primers located on the *WUS* locus.
(d) 3C-qPCR examining the *WUS* chromatin loop in L*er* and *wus-18*. Error bars represent SDs from three biological repeats. Gel imaging of the 3C-PCR result is presented in the insert. LC: loading control.
For panles (b)–(d), the inflorescences containing stage-8 and younger flowers of indicated plants were collected for the 3C assay. Crosslinked and non-crosslinked samples were used and the PCR with the A2 + D5 primer set served as a low interaction frequency control (d). Error bars represent SDs from three biological repeats. $^{**}P < 0.01$.

samples (Figure S3a, b). PCR with the A1 and A2 anchor primer set but not with other primer combinations produced a clear and specific band in the crosslinked samples, indicative of a specific DNA fragment containing sequences from the *WUS* 5′ TSS and *WUS* 3′ CRE regions (Figure S3a and S3b). qPCR was performed to examine the relative chromatin loop frequency (relative interaction frequency; see EXPERIMENTAL PROCEDURES) in the 3C DNA preparations. There was significant enrichment with the A1 and A2 anchor primer set over the other primer sets, whose lower levels reflected nonspecific amplification or random collisions, indicating that a chromatin loop brings the *WUS* 5′-TSS and *WUS* 3′-CRE regions within close proximity (Figure 1b and 1c). Sequencing of the PCR product showed the expected chimeric 3C product (Figure S4), helping to confirm that there are frequent physical interactions between the *WUS* 5′-TSS and *WUS* 3′-CRE regions *in vivo*. To confirm the existence of the *WUS* chromatin loop, we used another restriction enzyme (*Nla*III) to repeat the 3C experiment as described above. A specific 3C product with the A1 and A3 anchor primer set, but not with other primer combinations, was produced in the crosslinking samples (Figure S3c–g), providing solid evidence that the *WUS* 5′-TSS region interacts with the *WUS* 3′-CRE region.

We previously showed that the CArG boxes in the *WUS* 3′-CRE region are important for *WUS* expression regulation (Liu *et al.*, 2011). To dissect the role of the *WUS* 3′-CRE region in chromatin loop formation, we generated several *WUS* 3′-CRE-targeted knock-out lines using the clustered regularly interspaced short palindromic repeats (CRISPR)/Cas9 system (Shan *et al.*, 2014). PCR screening identified three individual lines containing an approximately 80-bp deletion at the target region, and DNA sequencing confirmed that the deletion segment included the tandem CArG boxes (Figure S5a, b). The individual line used for the 3C assay was named *wus-18*. Using the A1 and A2 anchor primer set, both PCR and qPCR assays detected dramatically decreased chromatin loop formation at the *WUS* locus in *wus-18*, compared with L*er*, indicating that the *WUS* 3′-CRE region containing the CArG boxes is critical for chromatin loop formation (Figure 1d). For these experiments, the A2 and D5 primer set (Figure 1a) served as a negative control (i.e. with low interaction frequency).

WUS 5′-TSS and *WUS* 3′-CRE regions are sufficient and necessary for chromatin loop formation

To investigate the function of *WUS* 5′-TSS and *WUS* 3′-CRE in *WUS* chromation loop formation, we designed a series of constructs in which the *WUS* distal promoter and coding region were replaced by the *35S* promoter and *GUS* reporter gene, respectively, with the following regions preserved: both *WUS* 5′-TSS and *WUS* 3′-CRE (construct C-I), *WUS* 5′-TSS only (construct C-II), *WUS* 3′-CRE only (construct C-III) or both regions, but with mutated CArG boxes (construct C-IV) (Figure 2a). The potential initiation codon ATG and one *Dpn*II site (GATC) in the 5′-UTR of the *WUS* gene were mutated in the constructs (Figure S6a). Finally, the constructs were named as *35S-WUS 5′:GUS:WUS 3′-CRE*, *35S-WUS 5′:GUS*, *35S:GUS:WUS 3′-CRE* and *35S-WUS 5′:GUS:WUS 3′-CREm*, respectively (Figure S6a). For each construct, we generated more than 30 individual single T-DNA insertion lines, and the integrity of the transgenic insert was confirmed (Figure S7). In the transgenic plants with GUS activity, specific primers for amplification of the 3C ligated product were designed for chromatin loop detection at *GUS* (Figure 2a). We then examined the chromatin loop formation at the *GUS* locus in a representative transgenic plant for each construct, and the *WUS* chromatin loop served as the internal control. C-I transgenic plants harbored a chromatin loop at the *GUS* locus, whereas C-II and C-III plants did not (Figure 2b), and the 3C product was confirmed by DNA sequencing (Figure S6b). For C-IV transgenic plants containing mutated CArG boxes, a weak chromatin interaction was detected, indicating that the CArG boxes are important for chromatin loop formation, but apparently not completely deleterious when mutated (Figure 2b). Interestingly, the presence of the T-DNA insertion in the *WUS* 3′-UTR in SALK_114398 failed to disrupt or even reduce the chromatin loop formation, suggesting that to some degree this conformation change at *WUS* is independent of the intervening physical distance (Figures 2c and S1a).

AG physically interacts with TFL2

Considering the co-localization of TFL2 and AG at the *WUS* 5′-TSS and *WUS* 3′-CRE regions, and the dependency of TFL2 binding to *WUS* on AG (Liu *et al.*, 2011), we sought to examine whether TFL2 and AG directly interact. TFL2 protein contains two related functional domains: an N-terminal chromodomain (CD) and a C-terminal chromo shadow domain (CSD) that are responsible for the binding of TFL2/LHP1 to methylated H3 and the positioning and stabilization of TFL2/LHP1 within the nucleolus, respectively (Zemach *et al.*, 2006). The MADS-domain protein AG is composed of the four following domains: the DNA-binding MADS domain (M), an intervening domain (I), a keratin-like domain (K) and a C-terminal domain (C) (Figure 3a; Kaufmann *et al.*, 2005). For the TFL2–AG interaction analysis, we conducted glutathione *S*-transferase (GST) pull-down assays using beads coated with purified His-TFL2 (1–445 AA) as the trapped protein, and GST, GST-AG (1–252 AA), GST-AG-MIK (1–195 AA) and GST-AG-C (195–252 AA) as the trapping proteins (Figure 3a). His-TFL2 directly bound to GST-AG and GST-AG-MIK, but not to GST alone or GST-AG-C (Figure 3b).

To provide additional evidence for the TFL2–AG interaction and to investigate the domains involved in the

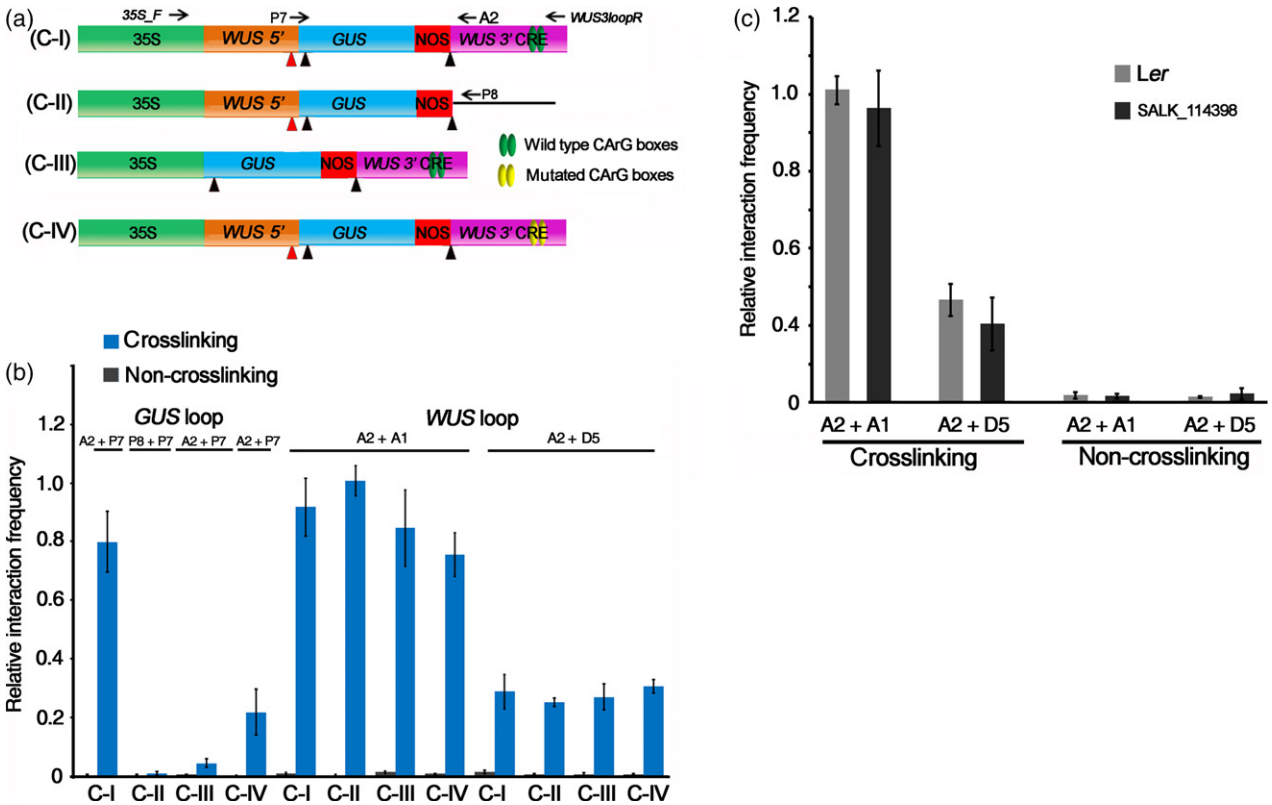

Figure 2. *WUS* 5′-TSS and *WUS* 3′-CRE regions are sufficient and necessary for chromatin loop formation.
(a) Schematic representation of the *GUS* reporter constructs used in this study. Native and mutated *Dpn*II sites are marked by black and red triangles, respectively. Wild-type CArG boxes and mutated CArG boxes are marked in green and yellow, respectively. To specifically amplify the 3C product from the *GUS* locus, primer P7, which spans the junction of the *WUS* 5′-TSS and the *GUS* coding region, was combined with the A2 or P8 primers used for the 3C assay. The primer locations are shown above the constructs.
(b) 3C-qPCR examining the chromatin loops at the *GUS* and *WUS* loci in the indicated representative transgenic plants for each of the indicated constructs in panel (a).
(c) 3C-qPCR examining the *WUS* chromatin loop in L*er* and SALK_114398. Error bars represent SDs from three biological repeats.

protein–protein interaction, we took advantage of a well-established yeast two-hybrid system to test the interaction between TFL2 and its binding proteins (Xu *et al.*, 2003; Li *et al.*, 2016). The pGADT7-TFL2/LHP1, pGADT7-TFL2/LHP1-N (1–194 AA), pGADT7-TFL2/LHP1-C (160–445 AA) and pGADT7-TFL2/LHP1-CSD (376–445 AA) constructs were described previously (Gaudin *et al.*, 2001; Li *et al.*, 2016). We generated the pGBKT7-AG, pGBKT7-AG-MIK, pGBKT7-AG-M (1–104 AA), pGBKT7-AG-IK (104–195 AA) and pGBKT7-AG-C (195–252 AA) constructs (Figure 3a). The yeast two-hybrid results showed that the C domain of AG had transactivation activity, indicative of its transcriptional activation function (Honma and Goto, 2001; de Folter *et al.*, 2005). Although the TFL2-N and AG-M domains were not involved in the TFL2–AG interaction, the C-terminal of TFL2 and the IK domains of AG were responsible for the TFL2–AG interaction; moreover, the CSD domain of TFL2 was sufficient for the interaction (Figure 3c). To confirm the TFL2–AG interaction *in planta*, we performed a co-immunoprecipitation (Co-IP) assay using *AG:AG-GFP 35S:TFL2-10xMyc* inflorescences. Anti-Myc and anti-GFP antibodies were used to precipitate the protein complexes containing TFL2-Myc and AG-GFP, respectively, followed by western blotting with anti-GFP and anti-Myc to detect the TFL2–AG interaction. As shown in Figure 3d and Figure S8, TFL2-Myc and AG-GFP were able to precipitate each other *in planta*. These results indicate that AG physically interacts with TFL2.

AG directly promotes *WUS* chromatin loop formation during flower development

During flower development, *WUS* expression peaks at stage 3 when *AG* expression begins, and is terminated at stage 6 by AG and other regulators, resulting in floral determinacy (Liu *et al.*, 2011; Cao *et al.*, 2015). To investigate the formation and function of the *WUS* chromatin loop in flower development, we used the established *35S:AP1-GR ap1 cal* line that allows the induction of synchronized flower development under dexamethasone (DEX) treatment (Wellmer *et al.*, 2006). We treated *35S:AP1-GR ap1 cal* inflorescences with DEX as previously described (Wellmer *et al.*, 2006), and collected tissues with

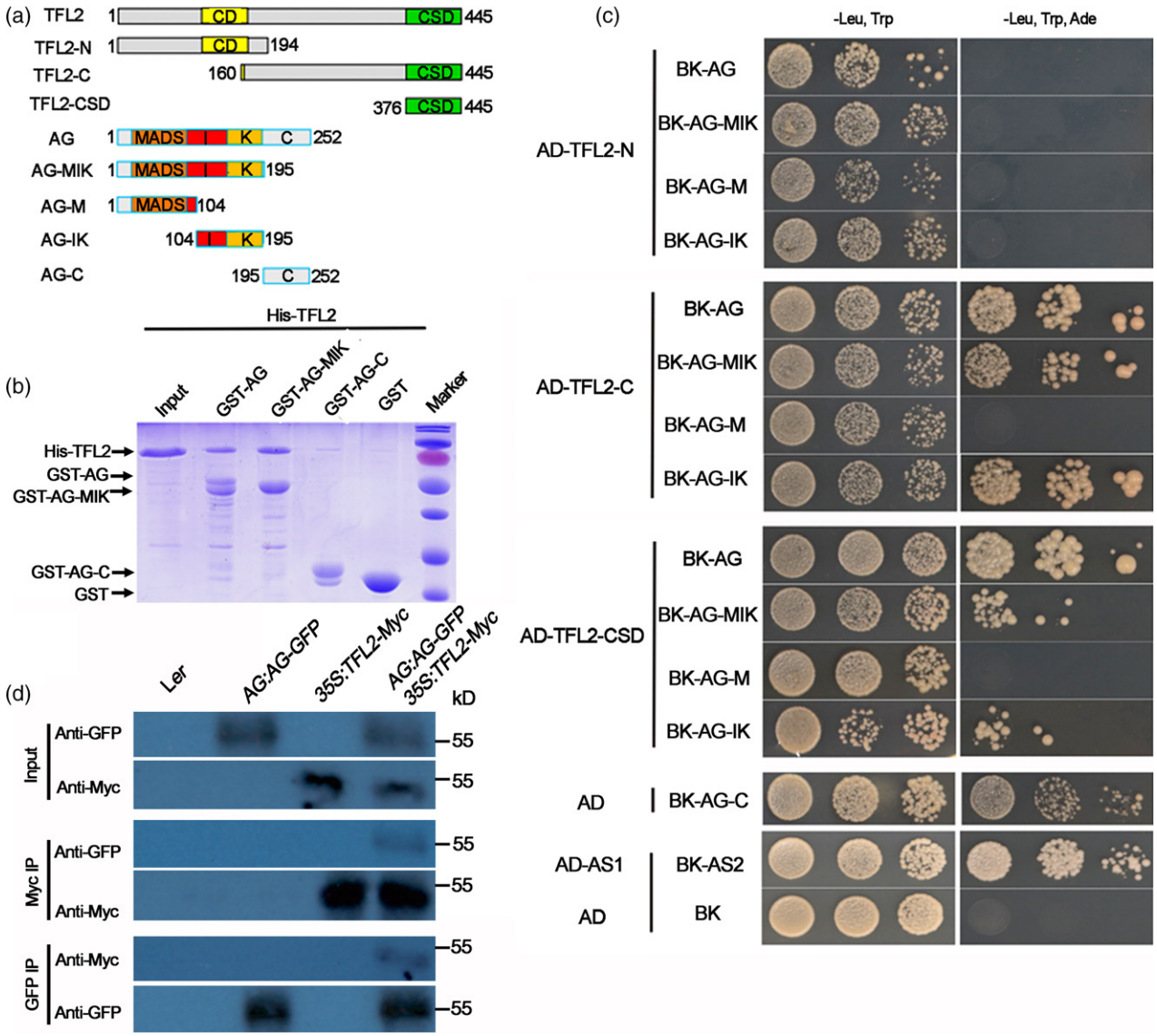

Figure 3. AG physically interacts with TFL2.

(a) Diagram of the TFL2 and AG functional domains. TFL2 contains two domains: the chromodomain (CD, yellow) and chromo shadow domain (CSD, green). The AG domains are as follows: MADS box (orange); the intervening domain (I, red); the keratin-like domain (K, gold); and the C-terminal domain (C, gray). The amino acid numbers of proteins used in the yeast two-hybrid analysis and pull-down assays are labeled.

(b) GST pull-down assay to examine the TFL2–AG interaction. Purified His-tagged TFL2 was incubated with an equal quantity of beads coated with GST, GST-AG, GST-AG-MIK and GST-AG-C. The GST protein was used as the negative control. The target proteins are marked on the left.

(c) Interaction between the functional domains of AG and TFL2 in the yeast two-hybrid assay. The indicated subdomains of TFL2 and AG were ligated into AD and BD vectors, respectively. The indicated combinations were co-transformed into yeast cells and screened on plates containing SD/–Leu,–Trp and SD/–Leu,–Trp,–Ade media. BK-AG-C has self-activity. AD-AS1 + BK-AS2 and AD + BD served as the positive and negative controls, respectively. AG-M: AG-MADS.

(d) Co-IP assay to examine AG-TFL2 interaction *in planta*. Total proteins were extracted, and western blotting was performed using anti-GFP and anti-Myc for the input control. Nucleic proteins from the inflorescences of the indicated plants were extracted. Anti-Myc and anti-GFP antibodies were used first for IP, then anti-GFP and anti-Myc were used to examine the AG-TFL2 interaction, respectively. Protein markers are labeled to the right. Four biological replicates gave similar results.

meristematic cells on days 0, 2 and 4 after treatment. The 3C assay revealed that *WUS* chromatin loop formation was increased after DEX treatment (Figure 4a). Decreased *WUS* expression under the same treatment suggested that the *WUS* chromatin loop may repress *WUS* expression during flower development (Figure S9) (Wellmer *et al.*, 2006). We next analyzed AG function in *WUS* chromatin loop formation using the *ag-1* null mutant. L*er* inflorescences containing stage-8 and younger flowers and *ag-1* inflorescences containing unopened flowers were collected for the 3C assay. We detected a significant reduction in chromatin loop formation in *ag-1* flowers compared with L*er*,

indicating a positive effect of *AG* on *WUS* chromatin loop formation (Figure 4b). We then used the *35S:AG-GR ag-1* system to determine whether the effect is direct, in light of the previous finding that AG could directly repress *WUS* expression after 2 h of AG induction (Liu *et al.*, 2011). After 2 h of treatment with DEX plus the protein synthesis inhibitor cycloheximide (CHX), with CHX alone as the control, a detectable and reproducible increase in *WUS* chromatin loop formation was triggered, and the increase was more significant after 6 h of treatment (Figure 4c). These findings indicated that AG promotes *WUS* chromatin loop formation directly.

To investigate whether AG binding to the *WUS* 5′-TSS region depends on the chromatin loop, we introduced the *AG:AG-GFP* transgene, which fully rescues the developmental defects of *ag-1* (Ji *et al.*, 2011), into *wus-18* by crossing. A chromatin immunoprecipitation (ChIP) assay with anti-GFP antibody was performed to examine AG occupancy at the *WUS* 5′-TSS and *WUS* 3′-CRE regions. AG enrichment at both regions was strikingly reduced in

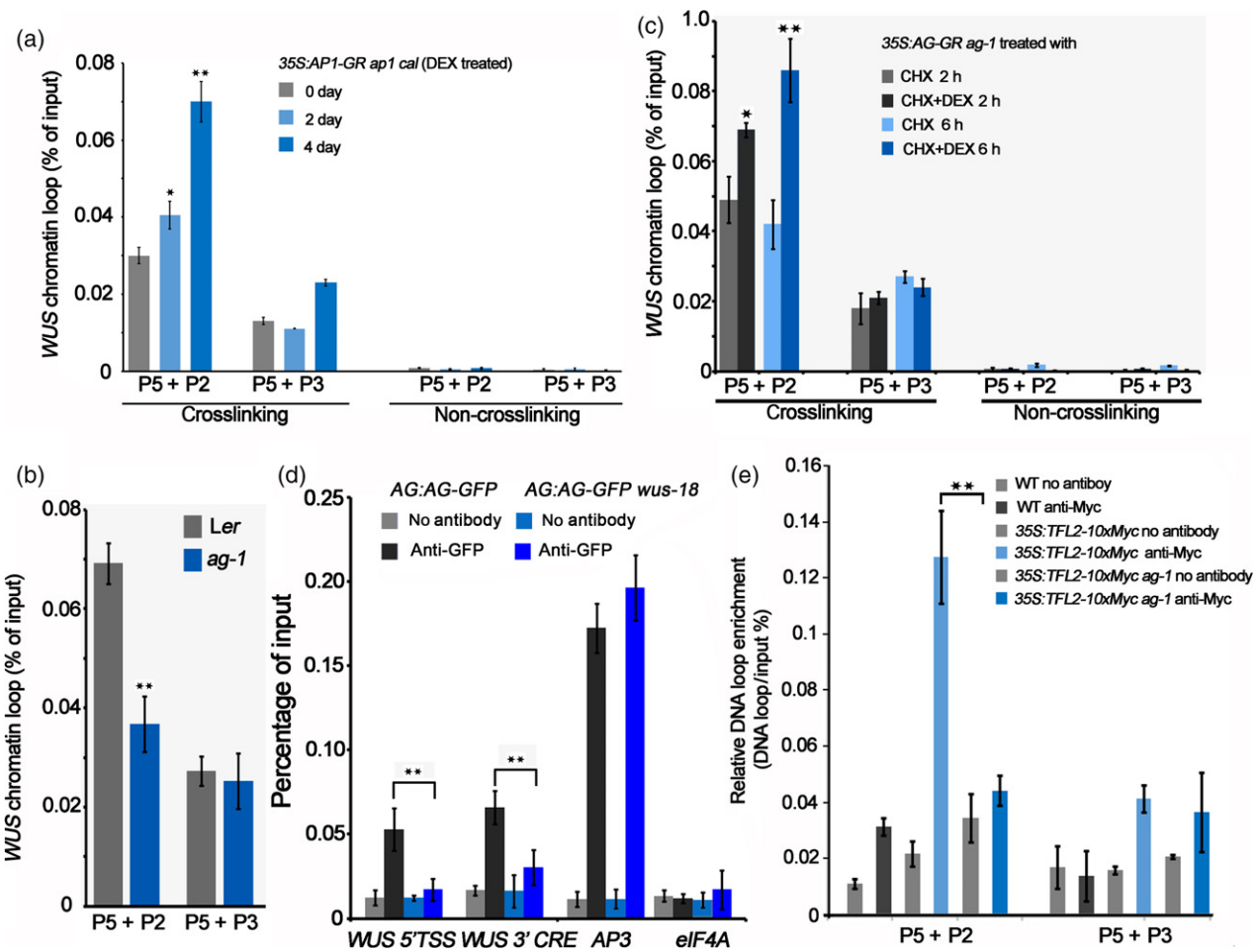

Figure 4. AG directly promotes *WUS* chromatin loop formation.

(a) *WUS* chromatin loop formation in *35S:AP1-GR ap1 cal* under DEX treatment. Inflorescences were treated with DEX to induce flower development and collected at the indicated time points for the 3C-qPCR assay.

(b) *WUS* chromatin loop formation in *ag-1*. Inflorescences containing stage-8 and younger flowers in L*er* and unopened flowers in *ag-1* were collected for the 3C-qPCR assay.

(c) *WUS* chromatin loop formation in *35S:AG-GR ag-1* under chemical treatment. Inflorescences were treated with the indicated chemicals for 2 h, and inflorescences containing stage-8 and younger flowers were collected for the 3C-qPCR assay. Crosslinked and non-crosslinked samples were used (a, c) and the PCR with the A2 + D5 primer set served as a low interaction frequency control. Error bars represent SDs from five biological replicates (a–c). $*P < 0.05$ and $**p < 0.01$.

(d) ChIP-qPCR using anti-GFP antibodies to determine AG occupancy at the *WUS* 5′-TSS and *WUS* 3′-CRE regions. *AG:AG-GFP* and *AG:AG-GFP wus-18* inflorescences were used for the ChIP assay. No antibody and the *eIF4A* locus both served as negative controls. *AP3*, a known direct target of AG (Gomez-Mena *et al.*, 2005), served as a positive control.

(e) ChIP-3C to examine *WUS* chromatin loop formation. Inflorescences containing stage-8 and younger flowers were collected from the indicated plants. The ChIP assay was performed using anti-Myc antibody, followed by a 3C assay. No antibody served as the negative control. Error bars represent SDs from four biological replicates (d, e). $**P < 0.01$.

AG:AG-GFP wus-18 compared with *AG:AG-GFP* (Figure 4d), indicating that the CArG boxes in the *WUS* 3′-CRE region are important for AG binding to the *WUS* 5′-TSS. In other words, AG binding to the *WUS* 5′-TSS appears to depend on the chromatin loop; however, we cannot tell whether AG directly binds to *WUS* 5′-TSS or indirectly binds to *WUS* through the interaction between AG and TFL2.

Our previous findings from a study of *TOP1*α revealed that a mutation in *TOP1*α led to increased nucleosome density at the *WUS* locus, which blocked AG binding to *WUS* and subsequently impaired FM determinacy (Liu *et al.*, 2014). We performed 3C-qPCR and qPCR assays using inflorescence tissue and found reduced *WUS* chromatin loop formation and increased *WUS* transcripts in the *top1*α mutant relative to the WT (Figure S10a, b). These findings further suggest that AG binding to the *WUS* 3′-CRE region is required for the formation of the *WUS* chromatin loop.

As AG physically interacts with TFL2 and is required for TFL2 binding to *WUS* (Figures 3b–d and S11; Liu *et al.*, 2011), we used the ChIP-3C technique to further investigate the role of the AG–TFL2 complex in *WUS* chromatin loop formation. Using *35S:TFL2-10xMyc* inflorescences containing stage-8 and younger flowers, we purified the TFL2-Myc fusion protein with anti-Myc antibody after crosslinking, sonication and IP, followed by a 3C experiment. A dramatic enrichment of the *WUS* chromatin loop was detected in the anti-Myc antibody output, compared with the no-antibody and WT controls (Figure 4e). *35S:TFL2-10xMyc* was also introduced into the *ag-1* background by crossing to examine the role of AG in TFL2/AG-mediated *WUS* chromatin loop formation. In the *ag-1* background, the ChIP-3C assay revealed a significant reduction in the enrichment of the *WUS* chromatin loop associated with TFL2 relative to the WT background (Figure 4e). In aggregate, these results indicate that TFL2-AG may directly promote *WUS* chromatin loop formation, and that AG is required for the function of TFL2 in this process.

The *WUS* chromatin loop represses gene expression

Several of the findings described above indicate that the *WUS* chromatin loop may inhibit *WUS* expression (Figures S9 and S10). To test this hypothesis, we examined *WUS* transcript levels and expression patterns in the *wus-18* plant. L*er* and *wus-18* inflorescences containing stage-8 and younger flowers were collected. qPCR revealed derepressed *WUS* transcript levels in *wus-18* compared with L*er* (Figure 5a), indicating that the *WUS* 3′-CRE mediates the regulation of *WUS* repression. To determine how the *WUS* 3′-CRE might regulate gene expression, we first examined the H3K27 m3 levels at the *WUS* 5′-TSS and *WUS* 3′-CRE regions in L*er* and *wus-18* inflorescences. H3K27 m3 enrichment in *wus-18* was similar to that in L*er* (Figure S12a). Thus, the deletion of the CArG boxes did not impair H3K27 m3 levels at these two regions; however, ChIP-qPCR revealed that TFL2 binding to the *WUS* 5′-TSS and *WUS* 3′-CRE regions was significantly reduced in the *wus-18* background compared with the WT background (Figure S12b). This finding was consistent with the reduced AG binding at these two regions in *wus-18* (Figure 4d) and the AG-dependent nature of TFL2 binding to *WUS* (Figure S11). We also examined nucleosome density at three sites in the *WUS* 5′-TSS region, the first intron and the *WUS* 3′-UTR (Figure S12c). This analysis was performed in L*er* and *wus-18* along with *top1*α, which was previously found to affect nucleosome density or positioning at the *WUS* locus (Liu *et al.*, 2014). The nucleosome density at both the *WUS* 5′-TSS and *WUS* 3′-UTR regions was reduced in *wus-18*, but was increased in *top1*α compared with L*er* (Figure S12c). No obvious differences in nucleosome density were detected at the *WUS* first intron site in L*er*, *wus-18* and *top1*α (Figure S12c). These findings indicate a looser chromatin structure at the *WUS* 5′-TSS and *WUS* 3′-UTR regions in *wus-18*, compared with L*er*, which is consistent with the higher *WUS* expression level in *wus-18* (Figure 5a).

In the early developing FM (stages 1–5) of L*er*, *WUS* expression is normally restricted and concentrated in the OC region, then shut off at stage 6 when carpel primordia are produced. Using the *WUS3.2:GUS:WUS3′mut* reporter line, in which *GUS* is driven by a partial *WUS* promoter (3.2 kb from the TSS), we previously found that mutations at the CArG boxes in the *WUS* 3′-CRE region prolonged *WUS* expression beyond stage 6 (Liu *et al.*, 2011). To examine the function of the chromatin loop in *WUS* expression regulation, we performed *in situ* hybridization in L*er* and *wus-18* flowers first, but we failed to detect any obvious differences in *WUS* expression patterns in stage-3 or stage-6 flowers between L*er* and *wus-18* (Figure S13). As *WUS* is critical for meristem maintenance and termination, any perturbed *WUS* expression will result in impaired meristem activity, resulting in meristem size alteration (Kinoshita *et al.*, 2010). We then examined the FM size of L*er* and *wus-18* flowers. The FM size of *wus-18* flowers at stage 3–4 was significantly larger than that in L*er* flowers (Figure 5b–d). As the L1 layer cells (the outermost layer of the FM) are clearly distinguished and the cell size was uniform throughout the layer between the central zone and peripheral zone (Laufs *et al.*, 1998), we counted the number of L1 layer cells in longitudinal FM sections by confocal imaging. *wus-18* flowers produced more L1 layer cells than L*er* flowers (20.5 ± 2.1 versus 15.2 ± 1.6; $n = 12$; Figure 5e), in line with the increased FM size in *wus-18* flowers.

As another strategy to investigate the function of the *WUS* chromatin loop in gene expression regulation, we next examined GUS activity, either by GUS staining or GUS activity quantification, in the different transgenic lines

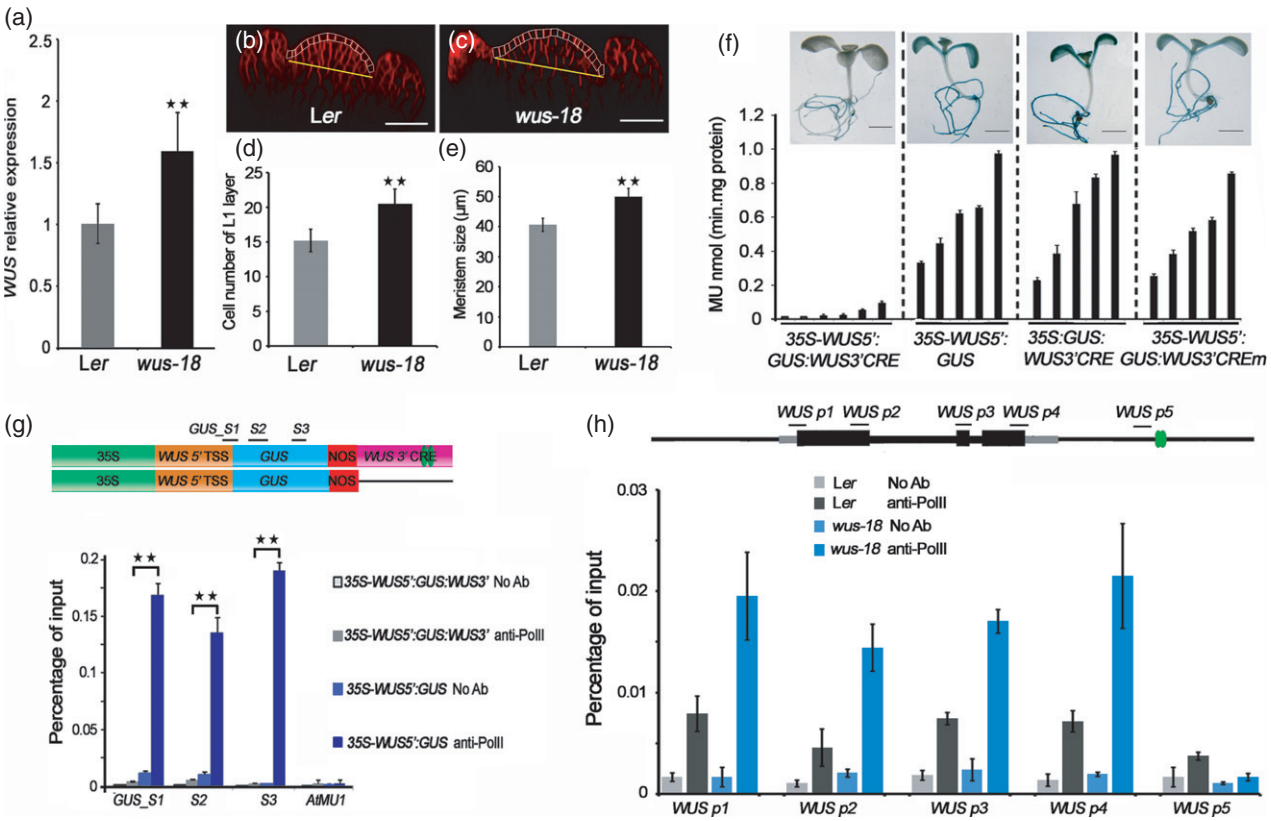

Figure 5. The *WUS* chromatin loop represses gene expression.
(a) qPCR experiment measuring *WUS* transcript levels in L*er* and *wus-18*. Inflorescences containing stage-8 and younger flowers were collected for the examination of *WUS* expression. Error bars represent SDs from three biological replicates. $^{**}P < 0.01$.
(b, c) Longitudinal sections of the inflorescence meristems of L*er* (b) and *wus-18* (c). Inflorescences containing stage-6 and younger flowers were stained with FM4-64 (red), and flowers at later stage 3 were selected for observation under a confocal microscope. Yellow lines mark the width of FM. The L1 layer cells are outlined in each panel. Scale bars: 20 μm.
(d) Quantification of floral meristem size (μm) of L*er* ($n = 15$) and *wus-18* (n = 15). $^{**}P < 0.01$.
(e) Number of cells in the FM L1 layer. The numbers of FM L1 layer cells in the indicated plants were counted, and the mean values from multiple flowers ($n = 12$) are shown. $^{**}P < 0.01$.
(f) GUS staining (upper panels) and β-glucuronidase quantitative analysis of the indicated transgenic plants. For each construct, several individual plants were selected and examined for the quantitative analysis. Error bars represent SDs from three biological replicates. Scale bars: 2 mm.
(g, h) ChIP analysis of Pol-II occupancy at the *GUS* locus (g) and *WUS* locus (h) in the indicated plants. The schematic diagrams show the regions examined by ChIP. In (g), anti-Pol II antibody was used to examine Pol-II occupancy at the *GUS* locus, with *AtMU1* as the negative control. Error bars represent SDs from three biological replicates. $^{**}P < 0.01$. In (h), anti-Pol II antibody was used to examine Pol-II occupancy at the whole *WUS* locus. Error bars represent SDs, which were calculated from three technical repeats. Three biological replicates gave similar results.

shown in Figure 2a. Transgenic plants with GUS activity that contained the intact chromatin loop (construct C-I) showed weak GUS staining signals, whereas plants that harbored *GUS* transgenes with compromised chromatin loop formation (constructs C-II, C-III and C-IV) produced clear and stronger GUS staining under the same histochemical staining conditions. For each transgenic construct, several independent lines were used for the quantitative GUS activity assay. The GUS activity in C-I plants was around 10 times less than that of plants with compromised chromatin loop formation (Figure 5f), indicating that the chromatin loop mediated by *WUS* 5′-TSS and *WUS* 3′-CRE inhibits the expression of the gene contained therein.

To investigate the molecular mechanism underlying the repression of chromatin loop on gene expression, we first examined the H3K27 m3 levels in the *GUS* transgenic plants, and in three randomly selected C-I and C-II individual lines. H3K27 m3 enrichment at the *GUS* locus was higher in C-II plants than in C-I plants (Figure S14a). TFL2 occupancy at the *GUS* locus was also investigated: we first introduced the *35S:TFL2-10Myc* transgene into the C-I and C-II plants used for the above H3K27 m3 enrichment assay, and ChIP-qPCR was performed with anti-Myc antibody. Surprisingly, TFL2 occupancy at the *GUS–S1* region (marked in Figure 5g) was lower in the C-II plants than in C-I plant (Figure S14b). These results indicate that TFL2 binding at the *GUS* locus was independent of the intensity

of H3K27 m3. RNA polymerase II (Pol II) pauses at promoter-proximal regions, and the release of paused Pol II permits elongation and productive gene transcription (Jonkers and Lis, 2015). To determine whether the *WUS* chromatin loop represses gene expression by disrupting Pol-II function, we performed ChIP-PCR to examine Pol-II occupancy at the *GUS* locus using an antibody against Pol II. In C-II transgenic plants, a high enrichment of Pol II was detected at both the promoter-proximal region and the coding region, in line with the high GUS activity observed in the plants. Conversely, in C-I plants with an intact chromatin loop at *GUS*, Pol II was rarely deposited at the *GUS* locus (Figure 5g), indicating that the chromatin loop may block the recruitment of Pol II to the target gene. Consistently, *GUS* mRNA transcript levels were significantly lower in C-I plants compared with the other transgenic plants (Figure S15). We also investigated the Pol-II occupancy at the *WUS* locus. Higher enrichment of Pol II at *WUS* in *wus-18* flowers than in L*er* flowers was detected, consistent with the increased *WUS* expression in *wus-18* inflorescences (Figures 5h and S16).

DISCUSSION

Chromatin loops were first characterized in yeast and subsequently reported in higher eukaryotes. The formation of chromatin loops usually results from promoter–enhancer or promoter–terminator interactions (O'Sullivan *et al.*, 2004; Ansari and Hampsey, 2005; Tan-Wong *et al.*, 2012). In plant cells, chromatin loops have recently been reported at several loci, including *FLOWERING LOCUS C* (*FLC*), *FLOWERING LOCUS T* (*FT*) and *PINOID* (*PID*) (Crevillen *et al.*, 2013; Ariel *et al.*, 2014; Cao *et al.*, 2014; Kim and Sung, 2017). At the *PID* locus, auxin signaling may open an existing chromatin loop within the long intergenic noncoding RNA (lincRNA) *AUXIN REGULATED PROMOTER LOOP* (*APOLO*) locus, thereby inducing *PID* and *APOLO* expression; subsequently, an *APOLO*–LHP1/TFL2 complex binds to the *PID* promoter to re-establish the repressive loop (Ariel *et al.*, 2014). In our study, we found that a chromatin loop exists at the *WUS* locus and is dependent on the interaction of two specific regions (Figures 1a–c and 2). One of the regions, *WUS* 3′-CRE, is beyond the *WUS* terminator, resulting in a chromatin loop similar to that reported for *FLC* (Crevillen *et al.*, 2013). Replacement of the *WUS* promoter and coding region with the *35S* promoter and *GUS* reporter gene, respectively, and a T-DNA insertion in the *WUS* 3′-UTR failed to disrupt chromatin loop formation. Taken together, the findings indicate that the *WUS* 5′-TSS and *WUS* 3′-CRE regions are necessary and sufficient for the formation of a chromatin loop in a manner independent of the sequence content of the intervening region and the genomic location (Figure 2). Moreover, the CArG boxes in the *WUS* 3′-CRE were important for chromatin loop formation and nucleosome density at the *WUS* locus, consistent with their role in the regulation of *WUS* expression (Figures 1d, 2b, 5a and S12c).

We could not determine whether TFL2 mediates *WUS* loop formation directly or simply binds to AG in the process of chromatin loop formation, because the *tfl2* mutant produces premature inflorescences. Nevertheless, our findings show that the *WUS* chromatin loop was directly mediated in part by AG, a MADS-domain TF important for floral organ identity and FM determinacy during flower development. It should be noted that TFL2 binds methylated H3, and that the *WUS* 5′-TSS region lacks a typical AG binding motif (Zemach *et al.*, 2006). Thus, the ability of AG to physically interact with TFL2/LHP1 (Figure 3) raises the possibility that an AG–TFL2 complex binds to the *WUS* 3′-CRE and *WUS* 5′-TSS regions through AG and TFL2, respectively, to promote *WUS* chromatin loop formation. This proposed mechanism is similar to that of the *APOLO*–LHP1/TFL2 complex in *PID* loop formation (Ariel *et al.*, 2014). We cannot rule out the possibility that other co-factors act with TFL2/AG to promote the formation of the *WUS* chromatin loop, however, because the binding of both AG and TFL2 to *WUS* was dramatically reduced rather than abolished in the *wus-18* mutant (Figures 4d and S12b).

The establishment of epigenetic gene repression by the PcG complex is often considered as a series of hierarchical events: PRC2 recruitment to the target locus; H3K27 trimethylation by the PRC2 complex; PRC1 recruitment to the target; and the repression of gene expression. Several studies have shown that PRC1 is required for PRC2 recruitment and H3K27 m3 modification, however (reviewed in Merini and Calonje, 2015). TFL2, the first proposed PRC1 component in plants, was recently found to regulate H3K27 m3 spreading and to shape local chromatin conformation to regulate target gene expression (Veluchamy *et al.*, 2016). Recent studies have also shown that TFL2 is required for H3K27 m3 deposition at target genes through direct interaction with specific TFs, such as ASYMMETRIC LEAVES 1 and 2 (AS1 and AS2) and SHORT VEGETATIVE PHASE (SVP) (Liu *et al.*, 2009; Li *et al.*, 2016). Here, we found that the TFL2 binding of *GUS* and *WUS* was independent of H3K27 m3 intensity; on the other hand, H3K27 m3 deposit was irrelevant to TFL2 occupancy at the target locus (Figures S12a, b and S14a, b). Interestingly, TFL2 binding to the *GUS* gene was lower in C-II plants than in C-I plants harboring an intact chromatin loop, raising the possibility that TFL2 involvement in regulating *WUS* is dependent on AG. Consistently, AG binding to *WUS* was CArG box-dependent, and TFL2 binding to *WUS* was AG-dependent (Figures 4d, S11 and S12b). In this context, our results provide further evidence of TFL2 mediating gene expression regulation in ways distinct from its function as a reader of the H3K27 m3 mark.

Chromatin loops resulting from promoter–terminator interaction have been proposed to promote Pol-II recycling

from the terminator to the promoter, and thus to facilitate transcription re-initiation (Lykke-Andersen *et al.*, 2011; Tan-Wong *et al.*, 2012). In Arabidopsis, local chromatin loops formed by the 5′ and 3′ ends of genes tend to occur in more highly expressed genes (Liu *et al.*, 2016). For example, the chromatin loop at the *FLC* locus that is released by BAF60 is required for maintaining *FLC* expression (Jegu *et al.*, 2014). In contrast, the chromatin loop at *WUS* or *GUS* repressed gene expression (Figure 5). Based on the reduced Pol-II occupancy at the *GUS* locus in C-I plants, compared with C-II plants, and at the *WUS* locus in L*er* plants, compared with *wus-18* (Figure 5g, h), *WUS* chromatin loop formation appeared to block the recruitment of Pol II to the gene. Given that the TSS site in the *WUS* 5′-TSS region is important for Pol-II recruitment, we hypothesized that chromatin loop formation triggers the condensation of local chromatin, resulting in the repression of transcription. This hypothesis is supported by the increased *WUS* expression level and the reduced nucleosome density at the *WUS* 5′-TSS region in the *wus-18* mutant (Figures 5a and S12c). Consistently, the line with a T-DNA insertion in the *WUS* 3′-UTR harbored a chromatin loop and displayed normal *WUS* transcript levels and expression patterns compared with the WT (Figure S1b, c). Although the chromatin loop was faintly detectable in C-IV transgenic plants with mutated CArG boxes (Figure 2b), C-IV plants nevertheless exhibited high GUS activity (Figure 5f), indicating that the de-repression of gene expression at this locus can still occur even if there are low levels of loop formation. On the other hand, chromatin loop-mediated *WUS* expression regulation is only one component of the multilayer regulatory network of this gene. Although GUS activity was dramatically prolonged with the constructs containing partial promoters (*WUS3.2:GUS:WUS3′mut* plants in Liu *et al.*, 2011), *wus-18* had only slightly higher *WUS* transcript levels and no expression pattern shift (Figures 5a and S13), underscoring that *WUS* expression regulation requires the coordinated interaction of multiple *trans*-acting factors and *cis*-acting elements (Baurle and Laux, 2005). In this context, our findings shed light on a new mechanism in which a specific TF, such as AG, interacts with TFL2 to promote local chromatin loop formation and alter local nucleosome density, resulting in gene expression regulation.

EXPERIMENTAL PROCEDURES

Plant materials and growth conditions

All plants are in the L*er* background, except for the *swn clf* mutant, *35S:TFL2-10xMyc* and the SALK_114398 line, which are in the Col background. Plants were grown in soil under long-day conditions (16-h light/8-h dark) at 23°C. The seeds of *swn/+ clf* were germinated on plates containing 1/2 × MS and 1% sucrose for 5 days, and seedlings with the *swn clf* phenotype were transplanted and grown on new MS plates for 2 weeks before sampling under long-day conditions. *ag-1*, *35S:AG-GR ag-1*, *35S:AP1-GR ap1 cal*, *top1α-2*, *35S:TFL2-10xMyc* and *tfl2-2* were described previously (Wellmer *et al.*, 2006; Liu *et al.*, 2011, 2014). The *WUS* T-DNA insertion mutant SALK_114398 was ordered from the Arabidopsis Biological Resource Center (ABRC, https://abrc.osu.edu), and the genotyping primers are listed in Table S1. Constructs C-I, C-II, C-III and C-IV were transformed into L*er*. DEX and CHX treatments were performed as previously described (Liu *et al.*, 2011).

Histochemical staining and β-glucuronidase quantitative analysis

For GUS staining, plant materials were immersed in GUS staining buffer (0.039 M $NaHPO_4$, 0.061 M Na_2HPO_4, 0.1 M EDTA, 0.0005 M *K*-ferricyanide, 0.0005 M *K*-ferrocyanide, 1% Triton, 0.25 mg ml^{-1} X-Gluc) and incubated for several hours in the dark at 37°C. The samples were washed with 70% ethanol until the chlorophyll was removed.

β-Glucuronidase quantitative analysis was performed as described by Zhang *et al.* (2018). Briefly, 0.05 g of plant material was ground into a fine powder in liquid N_2 and dissolved in 0.5 ml of protein extraction buffer. The supernatants were transferred to new tubes as total protein after the mixture was centrifuged. After the total protein concentration was determined by the BCA protein assay kit (#23227; ThermoFisher Scientific, https://www.thermofisher.com) and microplate procedure, 75 μl of total proteins, 300 μl of protein extraction buffer and 375 μl of 2 mM 4-methylumbelliferyl-β-D-glucuronide hydrate (M9130; Sigma-Aldrich, https://www.sigmaaldrich.com) were mixed and incubated at 37°C in the dark. The reaction was stopped at 0 min and 40 min by adding 900 μl of 0.2 M Na_2CO_3 to a 100-μl reaction mixture in a new tube, followed by an absorbance test at 360 nm of excitation length and 410 nm of emission length on a plate reader. A standard curve was made by serial dilution of 4-methylumbelliferone (MU) (M1381; Sigma-Aldrich) to determine the quantity of MU produced per minute for each sample tested. The quantity of MU generated per minute, which was normalized with total protein, was used to define GUS activity.

Plasmid construction

For the C-I construct, PCR was performed using the *WUS3loopF* and *WUS3loopR* primers and the *WUS3.2:GUS:WUS3′wt* plasmid (Liu *et al.*, 2011) as a template, to obtain the *WUS* 3′ CRE region fragment. The PCR product was digested with *Bam*HI and *Eco*RI, and the fragment was cloned into the destination vector *pPZP211* (Hajdukiewicz *et al.*, 1994), resulting in the *pPZP211-WUS3′CRE* vector. To amplify *WUS5′:GUS*, *WUS5loopF* and *GUS3loopR* were used with plasmid *WUS3.2:GUS:WUS3′wt* as a template. The PCR product digested with *Bam*HI was cloned into *pCambia99-1* (Zhao *et al.*, 2016) containing the cauliflower mosaic virus *35S* promoter and the NOS terminator. Sequencing was performed to ensure the integrity of the clone. Finally, *35S-WUS5′:GUS:NOS* was introduced into the vector *pPZP211-WUS3′CRE* by *Pst*I. To construct C-II, the *pCambia99-1* plasmid containing *35S-WUS5′:GUS:NOS* as described above was digested with *Pst*I for recombination into the destination vector *pPZP211*. For construct C-III, PCR was performed with the *GUS3loopF* and *GUS3loopR* primers and the *WUS3.2:GUS:WUS3′wt* plasmid as a template to obtain the *GUS* fragment. The PCR product was digested with *Apa*I and *Xba*I, and inserted into *pCambia99-1*, then cloned into the modified destination vector *pPZP211-WUS3′CRE* by *Pst*I. To construct C-IV, the mutated *WUS* 3′-CRE region fragment was obtained using

WUS3.2:GUS:WUS3′mut (Liu *et al.*, 2011) as a template and the same primer set used for the WT *WUS* 3′-CRE region fragment. The subsequent steps were identical to those described for the construction of C-I. The mutated sites were confirmed by sequencing. All primers used for vector construction are listed in Table S1.

3C and ChIP-3C assay

The 3C assay was performed as described previously (Hagege *et al.*, 2007; Louwers *et al.*, 2009), with some modifications. Plant chromatin was extracted as previously described (Liu *et al.*, 2011). Briefly, plant tissue was ground to a fine powder in liquid nitrogen and dissolved in M1 buffer [10 mM phosphate buffer, pH 7.0, 0.1 M NaCl, 10 mM β-mercaptoethanol, 1 M hexylene glycol (Sigma-Aldrich), 1× protease inhibitor cocktail (Roche, https://www.roche.com), and 1 mM phenylmethylsulfonyl fluoride (PMSF)], and then crosslinked with 1% formaldehyde (v/v%) for 10 min at 4°C, followed by quenching with 0.125 M glycine. The suspension was filtered through four layers of Miracloth, and the filtrate was centrifuged at 11 000 *g* for 10 min at 4°C. The supernatant was discarded and the pellet was washed three times with M2 buffer (M1 buffer plus 10 mM $MgCl_2$ and 0.5% Triton X-100), and once with M3 buffer [10 mM phosphate buffer, pH 7.0, 0.1 M NaCl, 10 mM mercaptoethanol, 1× protease inhibitor cocktail (Roche), and 1 mM PMSF]. After chromatin was extracted, it was washed one additional time with 400 μl of 1.2× *Dpn*II/*CutSmart* buffer and re-suspended with 500 μl of 1.2× *Dpn*II/*CutSmart* buffer. The subsequent steps were performed as described in Louwers *et al.* (2009). Briefly, the chromatin was digested with 100 units of *Dpn*II/*Nla*III overnight after pre-treatment with 0.3% SDS and 2% Triton X-100. Enzyme was inactivated by heating with 1.6% SDS. The chromatin was incubation with additional 375 μl of 20% Triton X-100 at 37°C in 7 ml 1× ligation buffer, which was followed by a ligation reaction for 10 h at 16°C. Chromatin was reverse crosslinked at 65°C with an additional 280 μl of 5 M NaCl for at least 6 h. After Proteinase K and RNase treatment, DNA was purified by phenol/chloroform extraction and precipitated with ethanol.

For ChIP-3C, ChIP was performed as previously described (Liu *et al.*, 2011) using anti-Myc antibody (ab32; Abcam, http://www.abcam.com). Chromatin was extracted as described above, until the M3 buffer wash. The pellet was re-suspended in nuclei lysis buffer [50 mM Tris-HCl, pH 8.0, 10 mM EDTA, 1% SDS, 1× protease inhibitor cocktail (Roche)]. Sonication was performed to generate DNA fragments around 500–1000 bp. The supernatant was diluted with ChIP dilution buffer [1.1% Triton X-100, 1.2 mM EDTA, 16.7 mM Tris-HCl, pH 8.0, 167 mM NaCl, 1× protease inhibitor cocktail (Roche)]. The diluted chromatin was pre-cleared by incubation with 50 μL of protein-A agarose beads/salmon sperm DNA (Millipore, now Merck, http://www.merckmillipore.com) for 1 h at 4°C, and then incubated with anti-Myc (ab32; Abcam) antibody overnight. A 150-μl volume of protein-A agarose beads was added to the chromatin mixture and incubated for 2 h at 4°C. The beads were washed with sequential buffers (twice for each buffer): low-salt buffer (150 mM NaCl, 0.1% SDS, 1% Triton X-100, 2 mM EDTA, 20 mM Tris-HCl, pH 8.0), high-salt buffer (500 mM NaCl, 0.1% SDS, 1% Triton X-100, 2 mM EDTA, 20 mM Tris-HCl, pH 8.0), LiCl buffer (0.25 mM LiCl, 1% NP-40, 1% sodium deoxycholate, 1 mM EDTA, 10 mM Tris-HCl, pH 8.0), and TE buffer (10 mM Tris-HCl, pH 8.0, 1 mM EDTA). Then nearly one-quarter of the beads were aliquoted into a new tube to reverse crosslink and purify DNA to test the ChIP efficiency, as described by Liu *et al.* (2011). The rest of the protein-A agarose beads bound to specific chromatin was washed with 400 μl of 1× *Dpn*II buffer once more, and then re-suspended with 200 μl of 1× *Dpn*II buffer. The 3C was performed as described above. Briefly, beads bound to specific chromatin were digested by *Dpn*II. After inactivation of *Dpn*II at 65°C, the ligation reaction was performed in 2 ml 1× ligation buffer. Then chromatin was reverse crosslinked and DNA was finally recovered. Real-time PCR was performed with the primers listed in Table S1.

3C quantification and normalization

3C quantification and normalization was performed as described in Crevillén *et al.* (2013), with modifications. A loading control (LC), in this case a primer set located on *WUS* genomic DNA that does not span the *Dpn*II/*Nla*III restriction site, was used for normalization because of the differences of DNA concentrations in the different samples.

To examine the amplification efficiency of each primer set, the whole genomic region of *WUS* was amplified with primers *T1* and *T2* by PCR in which the L*er* genomic DNA was used as a template. The PCR product was cloned into pENTR™/D-TOPO (Invitrogen, now ThermoFisher Scientific, https://www.thermofisher.com) and transformed into *Escherichia coli* strain JM110. Plasmids were extracted and digested by *Dpn*II/*Nla*III followed by subsequent ligation with serial dilutions (1, 1 : 2 and 1 : 4, corresponding to dilution-3, dilution-2 and dilution-1 samples), resulting in random ligations and all possible ligation products. C-I and C-II plasmids were also transformed into *E. coli* strain JM110 and equal molar volumes of C-I and C-II were mixed. *Dpn*II digestion and ligation was performed as described above. Primer pairs for *WUS* DNA loop and *GUS* DNA loop examination were used to test the primer efficiencies by real-time PCR, which was performed with the primers listed in Table S1.

To calculate the primer efficiency, all primer combinations in three dilution samples were normalized to the highest primer set in the dilution-1 sample to check whether the amplification efficiencies of different dilution samples showed the same trend. Then all primer combinations of each dilution sample were normalized to the highest primer set in its own dilution system. Finally, each primer efficiency was calculated as the average result from three dilutions.

To calculate the relative interaction frequency, three normalizations were performed. The 3C real-time PCR result was first normalized to sample the internal control 'LC'. To compensate for primer set efficiency, the first-normalized result was subsequently normalized to primer efficiency, here referred to as the 'second normalization result'. For all available primer sets using anchor primers with other primers located on *WUS*, the second normalization result was normalized to the highest primer set in the crosslinked sample. For comparing the 3C interaction between WT and mutants, the second normalization result was normalized to the (A2 + A1) result in the WT crosslinked sample. For comparing the *GUS* DNA loop in different transgenic plants, the second normalization result was normalized to the highest (A2 + A1) result of the *WUS* DNA loop in the crosslinked sample. For *35S:AP1-GR ap1 cal* and *35S:AG-GR ag-1*, the second normalization result was normalized to the highest (A2 + A1) result in the crosslinked sample.

ChIP assay

The ChIP assay was performed as previously described (Liu *et al.*, 2011). Briefly, the chromatin was extracted as described above using M1, M2 and M3 buffer. The lysate was pre-cleared with 50 μl of protein-A agarose beads/salmon sperm DNA (Millipore, now Merck) for 1 h, then incubated with anti-H3K27 m3 (07-449, Upstate, now Merck), anti-histone H3 (ab1791; Abcam), anti-Myc

(ab32; Abcam), anti-GFP (ab290; Abcam), or anti-PolII (ab817; Abcam) antibody overnight. The chromatin was purified using the Qiagen plasmid extraction kit according to the manufacturer's instructions. Real-time PCR was performed in triplicate.

Microscopy

Confocal images were recorded with a Leica TCS-SP8 confocal microscope as previously described (Zhang *et al.*, 2018). Plant membranes were visualized using FM4-64 at an excitation wave length of 561 nm and a detection wavelength of 570–620 nm.

CRISPR/Cas9-based gene editing

To simultaneously delete the two CArG boxes in the *WUS* gene, a pair of sgRNA targets (C0, 5′-ACTTTGCTGTAGGTTTTAA-3′, and C8, 5′-CAACTATTTTTATGCGGTT-3′) was designed. For the assembly of the two sgRNA sites, the PCR fragment was amplified from *pCBC-DT1T2* with primers *L0-BsF*, *L0-F0*, *L8-R0* and *L8-BsR* (Table S1). The PCR product was purified and digested with *Bsa*I then ligated into *Bsa*I-linearized *pHEE2A-TRI* (Wang *et al.*, 2015), resulting in the final deletion vector *pHEE2A-TRI-C0C8*, which was transformed into L*er* by *Agrobacterium tumefaciens* via floral dip (Clough and Bent, 1998). PCR reactions and sequencing were performed using the hygromycin-resistant transgenic plants.

RNA extraction and real-time quantitative PCR

Total RNA was isolated from Arabidopsis inflorescences or seedlings using the RNeasy plant mini kit (Qiagen, https://www.qiagen.com) and treated with DNase*I* (Roche) to eliminate DNA contamination. M-MLV Reverse Transcriptase (Promega, https://www.promega.com) was used for reverse transcription. Quantitative real-time RT-PCR was performed in triplicate on a Bio-Rad CFX-96 Real-time PCR system (Bio-Rad, http://www.bio-rad.com) using the SYBR Green RT-PCR kit (DBI Bioscience. Co., Ludwigshafen, Germany). For gene expression analysis, *UBQ5* served as the internal control. For relative DNA loop frequency and amplification efficiency testing of primer sets, the region flanking the *WUS* TSS (underlined in red in Figure 1a) amplified by primers P11 and P12 served as the input control.

Yeast two-hybrid and Co-IP assay

The pGADT7-AS1, pGBKT7-AS2, pGADT7-TFL2-N, pGADT7-TFL2-C and pGADT7-TFL2-CSD constructs were described previously (Xu *et al.*, 2003; Li *et al.*, 2016). *AG*, *AG-MIK*, *AG-M*, *AG-IK* and *AG-C* cDNAs were amplified and cloned into the *Eco*RI-*Sal*I sites of the PGADT7 vector (Clontech, http://www.clontech.com). The yeast two-hybrid assay was performed according to the manufacturer's protocol (Clontech).

Co-IP assays were performed as previously described (Li *et al.*, 2012), with some modifications. Inflorescences containing unopened flowers were collected and crosslinked with 1% formaldehyde, followed by nuclear extraction, as in the ChIP procedure described above (Liu *et al.*, 2014). The nuclei were digested with 0.4 U μl^{-1} micrococcal nuclease (NEB, https://www.neb.com) and incubated at 37°C for 30 min to completely digest the chromatin, as previously described (Liu *et al.*, 2014). The suspension was centrifuged at 12 000 *g* at 4°C for 5 min. The pellet was re-suspended with IP buffer, followed by sonication. Anti-*c*-Myc Magnetic Beads (Pierce, now ThermoFisher Scientific) or anti-GFP (Abcam) were added to precipitate the TFL2-Myc protein complex, and anti-GFP (Abcam) and anti-Myc (Abcam) were used to detect the AG–TFL2 interaction by western blotting.

Protein expression and pull-down assays

The pGEX-4T1-TFL2 and pET-28a-TFL2-CSD constructs were described previously (Li *et al.*, 2016). *AG*, *AG-MIK*, *AG-IK* and *AG-C* cDNAs were amplified and cloned into the *Eco*RI-*Sal*I sites of the pGEX-6p-1 vector to produce the GST-fused proteins. For the 6xHis-TFL2-C construct, the DNA fragment encoding TFL2-C was subcloned into the pET28a vector (Novagen, now Merck).

His-tag TFL2, TFL2-C and TFL2-CSD, and GST-tag AG, AG-MIK, AG-IK and AG-C recombinant proteins were expressed and purified as previously described (Li *et al.*, 2016). Pull-down experiments were also performed as previously described (Li *et al.*, 2016).

Micrococcal nuclease digestion of chromatin

Micrococcal nuclease (MNase) digestion was performed as previously described (Liu *et al.*, 2014), with some modifications. Briefly, chromatin was extracted as described above. After washing with M3 buffer, the chromatin was washed with MNase digestion buffer and re-suspended with digestion buffer [50 mM Tris-HCl, 5 mM $CaCl_2$, 1 × BSA, 20 mg ml^{-1} RNase A and 1 × protease inhibitor cocktail (Roche)] containing 0.1 U μl^{-1} micrococcal nuclease (ThermoFisher Scientific). The reaction was stopped at different digestion times (0, 5, 8 and 15 min) with equal volumes of lysis buffer (0.1 M Tris, pH 8.0, 0.1 M NaCl, 50 mM EDTA, 1% SDS, 0.2 mg ml^{-1} Proteinase K). After incubation at 45°C, DNA was extracted using the phenol/chloroform method and precipitated with ethanol. After RNase A treatment, purified DNA was resolved on a 2% agarose gel to check the digestion result. Real-time PCR was performed with primers located at the *WUS* 5′-TSS, the *WUS* 3′-CRE and the first intron, as shown in Figure S12c. All primers used are listed in Table S1.

In situ hybridization

In situ hybridization was performed as previously described (Liu *et al.*, 2011). The pGEM-T-easy (Promega) plasmid harboring the *WUS* coding region was digested with *Spe*I and transcribed with T7 RNA polymerase to generate the antisense probe for *WUS*. The floral developmental stages were as described by Smyth *et al.* (1990).

ACCESSION NUMBERS

Sequence data from this article can be found in the GenBank/EMBL data libraries under the following accession numbers: *AG*, AT4G18960; *AP3*,AT3G54340; *CLF*, AT2G23380; *eIF4A*, AT3G13920; *SWN*, AT4G02020; *TFL2/LHP1*, AT5G17690; *TOP1a*, AT5G55300; *UBQ5*, AT3G62250; and *WUS*, AT2G17950.

ACKNOWLEDGEMENTS

We thank Xuemei Chen and Rae Eden Yumul for comments on the manuscript and Hao Yu for valuable advice on the 3C technique. This work was funded by the National Science Foundation of China (NSFC) Project 31671354, National Basic Research Program of China Grant 2014CB138100 and CAS Pioneer Hundred Talents Program (to X.L.) and NSFC Grant 31401039 (to L.G.).

CONFLICT OF INTEREST

The authors declare that they have no competing interests.

AUTHOR CONTRIBUTIONS

L.G. and X.L. conceived and designed the study. L.G., X.C., Y.L., K.Z. and D.L. performed most of experiments, with

the help of Y.L. and A.D in protein–protein interaction and J.L. and C.G. in CRISPR/Cas9-based gene editing. L.G., A.D., C.G. and X.L. analyzed the data. L.G., Y.L., J.L. and X.L. wrote the manuscript.

SUPPORTING INFORMATION

Additional Supporting Information may be found in the online version of this article.

Figure S1. *WUS* transcript levels and expression patterns were unaffected by a T-DNA insertion in the *WUS* 3′-UTR.

Figure S2. Amplification efficiency testing of primer sets used in the 3C assay.

Figure S3. Confirmation of the existence of *WUS* chromatin loop by 3C experiment with *Dpn*II and *Nla*III digestion.

Figure S4. Sequencing chromatogram showing the 3C PCR product using the A1 and A2 primers.

Figure S5. sgRNA:Cas9-induced *WUS* mutations in transgenic Arabidopsis plants.

Figure S6. *GUS* reporter gene constructs and 3C product sequencing.

Figure S7. Examination of insert integrity in the transgenic plants.

Figure S8. AG physically interacts with TFL2 *in planta*.

Figure S9. *WUS* expression in *35S:AP1-GR ap1 cal* plants under DEX treatment.

Figure S10. *WUS* chromatin loop and expression in the *top1α* mutant.

Figure S11. ChIP using anti-Myc antibody to examine TFL2 occupancy at *WUS* in *35S:TFL2-10xMyc* and *35S:TFL2-10xMyc ag-1* inflorescences.

Figure S12. H3K27 m3 levels, TFL2 binding to *WUS* and nucleosome density at the *WUS* locus in L*er* and *wus-18*.

Figure S13. *In situ* hybridization to detect *WUS* expression patterns in WT and *wus-18* plants.

Figure S14. H3K27 m3 levels and TFL2 occupancy at the *GUS* locus in transgenic plants.

Figure S15. *GUS* expression in transgenic plants.

Figure S16. ChIP analysis of Pol-II occupancy at the *WUS* locus.

Table S1. List of primers used in this study.

REFERENCES

Ansari, A. and Hampsey, M. (2005) A role for the CPF 3′-end processing machinery in RNAP II-dependent gene looping. *Genes Dev.* **19**, 2969–2978.

Ariel, F., Jegu, T., Latrasse, D., Romero-Barrios, N., Christ, A., Benhamed, M. and Crespi, M. (2014) Noncoding transcription by alternative RNA polymerases dynamically regulates an auxin-driven chromatin loop. *Mol. Cell*, **55**, 383–396.

Baurle, I. and Laux, T. (2005) Regulation of WUSCHEL transcription in the stem cell niche of the Arabidopsis shoot meristem. *Plant Cell*, **17**, 2271–2280.

Cao, S., Kumimoto, R.W., Gnesutta, N., Calogero, A.M., Mantovani, R. and Holt, B.F. 3rd (2014) A distal CCAAT/NUCLEAR FACTOR Y complex promotes chromatin looping at the FLOWERING LOCUS T promoter and regulates the timing of flowering in Arabidopsis. *Plant Cell*, **26**, 1009–1017.

Cao, X., He, Z., Guo, L. and Liu, X. (2015) Epigenetic mechanisms are critical for the regulation of WUSCHEL expression in floral meristems. *Plant Physiol.* **168**, 1189–1196.

Clough, S.J. and Bent, A.F. (1998) Floral dip: a simplified method for Agrobacterium-mediated transformation of Arabidopsis thaliana. *Plant J.* **16**, 735–743.

Crevillen, P., Sonmez, C., Wu, Z. and Dean, C. (2013) A gene loop containing the floral repressor FLC is disrupted in the early phase of vernalization. *The EMBO journal*, **32**, 140–148.

Dekker, J., Rippe, K., Dekker, M. and Kleckner, N. (2002) Capturing chromosome conformation. *Science (New York, N.Y.)*, **295**, 1306–1311.

de Folter, S., Immink, R.G., Kieffer, M. *et al.* (2005) Comprehensive interaction map of the Arabidopsis MADS Box transcription factors. *Plant Cell*, **17**, 1424–1433.

Gallois, J.L., Nora, F.R., Mizukami, Y. and Sablowski, R. (2004) WUSCHEL induces shoot stem cell activity and developmental plasticity in the root meristem. *Genes Dev.* **18**, 375–380.

Gaudin, V., Libault, M., Pouteau, S., Juul, T., Zhao, G., Lefebvre, D. and Grandjean, O. (2001) Mutations in LIKE HETEROCHROMATIN PROTEIN 1 affect flowering time and plant architecture in Arabidopsis. *Development*, **128**, 4847–4858.

Gomez-Diaz, E. and Corces, V.G. (2014) Architectural proteins: regulators of 3D genome organization in cell fate. *Trends Cell Biol.* **24**, 703–711.

Gomez-Mena, C., de Folter, S., Costa, M.M., Angenent, G.C. and Sablowski, R. (2005) Transcriptional program controlled by the floral homeotic gene AGAMOUS during early organogenesis. *Development*, **132**, 429–438.

Hagege, H., Klous, P., Braem, C., Splinter, E., Dekker, J., Cathala, G., de Laat, W. and Forne, T. (2007) Quantitative analysis of chromosome conformation capture assays (3C-qPCR). *Nat. Protoc.* **2**, 1722–1733.

Hajdukiewicz, P., Svab, Z. and Maliga, P. (1994) The small, versatile pPZP family of Agrobacterium binary vectors for plant transformation. *Plant Mol. Biol.* **25**, 989–994.

Honma, T. and Goto, K. (2001) Complexes of MADS-box proteins are sufficient to convert leaves into floral organs. *Nature*, **409**, 525–529.

Huang, H., Mizukami, Y., Hu, Y. and Ma, H. (1993) Isolation and characterization of the binding sequences for the product of the Arabidopsis floral homeotic gene AGAMOUS. *Nucleic Acids Res.* **21**, 4769–4776.

Jegu, T., Latrasse, D., Delarue, M., Hirt, H., Domenichini, S., Ariel, F., Crespi, M., Bergounioux, C., Raynaud, C. and Benhamed, M. (2014) The BAF60 subunit of the SWI/SNF chromatin-remodeling complex directly controls the formation of a gene loop at FLOWERING LOCUS C in Arabidopsis. *Plant Cell*, **26**, 538–551.

Ji, L.J., Liu, X.G., Yan, J. *et al.* (2011) ARGONAUTE10 and ARGONAUTE1 regulate the termination of floral stem cells through two MicroRNAs in arabidopsis. *PLoS Genet.* **7**(3), e1001358.

Jonkers, I. and Lis, J.T. (2015) Getting up to speed with transcription elongation by RNA polymerase II. *Nat. Rev. Mol. Cell Biol.* **16**, 167–177.

Kadauke, S. and Blobel, G.A. (2009) Chromatin loops in gene regulation. *Biochem. Biophys. Acta.* **1789**, 17–25.

Kaufmann, K., Melzer, R. and Theißen, G. (2005) MIKC-type MADS-domain proteins: structural modularity, protein interactions and network evolution in land plants. *Gene*, **347**, 183–198.

Kim, D.H. and Sung, S. (2017) Vernalization-triggered intragenic chromatin loop formation by long noncoding RNAs. *Dev. Cell*, **40**, e304.

Kinoshita, A., Betsuyaku, S., Osakabe, Y., Mizuno, S., Nagawa, S., Stahl, Y., Simon, R., Yamaguchi-Shinozaki, K., Fukuda, H. and Sawa, S. (2010) RPK2 is an essential receptor-like kinase that transmits the CLV3 signal in Arabidopsis. *Development*, **137**, 3911–3920.

Laufs, P., Grandjean, O., Jonak, C., Kiêu, K. and Traas, J. (1998) Cellular parameters of the shoot apical meristem in arabidopsis. *Plant Cell*, **10**, 1375–1389.

Laux, T., Mayer, K.F.X., Berger, J. and Jurgens, G. (1996) The WUSCHEL gene is required for shoot and floral meristem integrity in Arabidopsis. *Development*, **122**, 87–96.

Lenhard, M., Bohnert, A., Jurgens, G. and Laux, T. (2001) Termination of stem cell maintenance in Arabidopsis floral meristems by interactions between WUSCHEL and AGAMOUS. *Cell*, **105**, 805–814.

Li, Z., Li, B., Shen, W.H., Huang, H. and Dong, A. (2012) TCP transcription factors interact with AS2 in the repression of class-I KNOX genes in Arabidopsis thaliana. *Plant J.* **71**, 99–107.

Li, Y., Chen, C.Y., Kaye, A.M. and Wasserman, W.W. (2015) The identification of cis-regulatory elements: a review from a machine learning perspective. *Bio Systems*, **138**, 6–17.

Li, Z., Li, B., Liu, J. *et al.* (2016) Transcription factors AS1 and AS2 interact with LHP1 to repress KNOX genes in Arabidopsis. *J. Integr. Plant Biol.* **58**(12), 959–970.

Liu, C., Xi, W., Shen, L., Tan, C. and Yu, H. (2009) Regulation of floral patterning by flowering time genes. *Dev. Cell*, **16**, 711–722.

Liu, X.G., Kim, Y.J., Muller, R., Yumul, R.E., Liu, C.Y., Pan, Y.Y., Cao, X.F., Goodrich, J. and Chena, X.M. (2011) AGAMOUS terminates floral stem cell maintenance in arabidopsis by directly repressing WUSCHEL through recruitment of polycomb group proteins. *Plant Cell*, **23**, 3654–3670.

Liu, C., Teo, Z.W., Bi, Y., Song, S., Xi, W., Yang, X., Yin, Z. and Yu, H. (2013) A conserved genetic pathway determines inflorescence architecture in Arabidopsis and rice. *Dev. Cell*, **24**, 612–622.

Liu, X., Gao, L., Dinh, T.T., Shi, T., Li, D., Wang, R., Guo, L., Xiao, L. and Chen, X. (2014) DNA topoisomerase I affects polycomb group protein-mediated epigenetic regulation and plant development by altering nucleosome distribution in Arabidopsis. *Plant Cell*, **26**, 2803–2817.

Liu, C., Wang, C., Wang, G., Becker, C., Zaidem, M. and Weigel, D. (2016) Genome-wide analysis of chromatin packing in Arabidopsis thaliana at single-gene resolution. *Genome Res.* **26**, 1057–1068.

Louwers, M., Bader, R., Haring, M., van Driel, R., de Laat, W. and Stam, M. (2009) Tissue- and expression level-specific chromatin looping at maize b1 epialleles. *Plant Cell*, **21**, 832–842.

Lykke-Andersen, S., Mapendano, C.K. and Jensen, T.H. (2011) An ending is a new beginning: transcription termination supports re-initiation. *Cell cycle (Georgetown, Tex.)*, **10**, 863–865.

Matharu, N. and Ahituv, N. (2015) Minor loops in major folds: enhancer–promoter looping, chromatin restructuring, and their association with transcriptional regulation and disease. *PLoS Genet.* **11**, e1005640.

Mattout, A. and Meshorer, E. (2010) Chromatin plasticity and genome organization in pluripotent embryonic stem cells. *Curr. Opin. Cell Biol.* **22**, 334–341.

Mayer, K.F.X., Schoof, H., Haecker, A., Lenhard, M., Jurgens, G. and Laux, T. (1998) Role of WUSCHEL in regulating stem cell fate in the Arabidopsis shoot meristem. *Cell*, **95**, 805–815.

Merini, W. and Calonje, M. (2015) PRC1 is taking the lead in PcG repression. *Plant J.* **83**, 110–120.

O'Sullivan, J.M., Tan-Wong, S.M., Morillon, A., Lee, B., Coles, J., Mellor, J. and Proudfoot, N.J. (2004) Gene loops juxtapose promoters and terminators in yeast. *Nat. Genet.* **36**, 1014–1018.

Prunet, N., Morel, P., Negrutiu, I. and Trehin, C. (2009) Time to stop: flower meristem termination. *Plant Physiol.* **150**, 1764–1772.

Sablowski, R. (2007) Flowering and determinacy in Arabidopsis. *J. Exp. Bot.* **58**, 899–907.

Scheres, B. (2007) Stem-cell niches: nursery rhymes across kingdoms. *Nat. Rev. Mol. Cell Biol.* **8**, 345–354.

Shan, Q., Wang, Y., Li, J. and Gao, C. (2014) Genome editing in rice and wheat using the CRISPR/Cas system. *Nat. Protoc.* **9**, 2395–2410.

Shiraishi, H., Okada, K. and Shimura, Y. (1993) Nucleotide sequences recognized by the AGAMOUS MADS domain of Arabidopsis thaliana in vitro. *Plant J.* **4**, 385–398.

Smaczniak, C., Immink, R.G., Muino, J.M. *et al.* (2012) Characterization of MADS-domain transcription factor complexes in Arabidopsis flower development. *Proc Natl Acad Sci U S A*, **109**, 1560–1565.

Smyth, D.R., Bowman, J.L. and Meyerowitz, E.M. (1990) Early flower development in arabidopsis. *Plant Cell*, **2**, 755–767.

Sun, B. and Ito, T. (2015) Regulation of floral stem cell termination in Arabidopsis. *Front Plant Sci.* **6**, 17.

Sun, B., Xu, Y.F., Ng, K.H. and Ito, T. (2009) A timing mechanism for stem cell maintenance and differentiation in the Arabidopsis floral meristem. *Genes Dev.* **23**, 1791–1804.

Sun, B., Looi, L.S., Guo, S., He, Z., Gan, E.S., Huang, J., Xu, Y., Wee, W.Y. and Ito, T. (2014) Timing mechanism dependent on cell division is invoked by Polycomb eviction in plant stem cells. *Science (New York, N.Y.)*, **343**, 1248559.

Tan-Wong, S.M., Zaugg, J.B., Camblong, J., Xu, Z., Zhang, D.W., Mischo, H.E., Ansari, A.Z., Luscombe, N.M., Steinmetz, L.M. and Proudfoot, N.J. (2012) Gene loops enhance transcriptional directionality. *Science (New York, N.Y.)*, **338**, 671–675.

Veluchamy, A., Jegu, T., Ariel, F. *et al.* (2016) LHP1 Regulates H3K27me3 spreading and shapes the three-dimensional conformation of the arabidopsis genome. *PLoS ONE*, **11**, e0158936.

Wang, Z.P., Xing, H.L., Dong, L., Zhang, H.Y., Han, C.Y., Wang, X.C. and Chen, Q.J. (2015) Egg cell-specific promoter-controlled CRISPR/Cas9 efficiently generates homozygous mutants for multiple target genes in Arabidopsis in a single generation. *Genome Biol.* **16**, 144.

Wellmer, F., Alves-Ferreira, M., Dubois, A., Riechmann, J.L. and Meyerowitz, E.M. (2006) Genome-wide analysis of gene expression during early Arabidopsis flower development. *PLoS Genet.* **2**, e117.

Xu, L., Xu, Y., Dong, A., Sun, Y., Pi, L., Xu, Y. and Huang, H. (2003) Novel as1 and as2 defects in leaf adaxial-abaxial polarity reveal the requirement for ASYMMETRIC LEAVES1 and 2 and ERECTA functions in specifying leaf adaxial identity. *Development*, **130**, 4097–4107.

Yanofsky, M.F., Ma, H., Bowman, J.L., Drews, G.N., Feldmann, K.A. and Meyerowitz, E.M. (1990) The protein encoded by the Arabidopsis homeotic gene agamous resembles transcription factors. *Nature*, **346**, 35–39.

Zemach, A., Li, Y., Ben-Meir, H., Oliva, M., Mosquna, A., Kiss, V., Avivi, Y., Ohad, N. and Grafi, G. (2006) Different domains control the localization and mobility of LIKE HETEROCHROMATIN PROTEIN1 in Arabidopsis nuclei. *Plant Cell*, **18**, 133–145.

Zhang, K., Wang, R., Zi, H. *et al.* (2018) AUXIN RESPONSE FACTOR3 regulates floral meristem determinacy by repressing cytokinin biosynthesis and signaling. *Plant Cell*, **30**(2), 324–346.

Zhao, Y., Chan, Z., Gao, J. *et al.* (2016) ABA receptor PYL9 promotes drought resistance and leaf senescence. *Proc Natl Acad Sci U S A*, **113**, 1949–1954.